Cerebellum Dysfunction in Patients With PRRT2-Related Paroxysmal Dyskinesia

Asya Ekmen, Aurelie Meneret, Romain Valabregue, Benoit Beranger, Yulia Worbe, Jean-Charles Lamy, Sofien Mehdi, Anais Herve, Isaac Adanyeguh, Gizem Temiz, et al.

Cerebellum dysfunction in patients with PRRT2-related paroxysmal dyskinesia

Author(s):

Asya Ekmen, MD[1]; Aurelie Meneret, MD, PhD[1, 2]; Romain Valabregue, PhD[1]; Benoit Beranger, BSc[1]; Yulia Worbe, MD, PhD[1]; Jean-Charles Lamy, PhD[1]; Sofien Mehdi, BTech[1]; Anais Herve, RN[1]; Isaac Adanyeguh, PhD[1, 3]; Gizem Temiz, BSc[1]; Philippe Damier, MD, PhD[4]; Domitille Gras, MD, PhD[5]; Agathe Roubertie, MD, PhD[6]; Juliette Piard, MD, PhD[7]; Vincent Navarro, MD, PhD[1, 2]; Eugenie Mutez, MD, PhD[8]; Florence Riant, MD, PhD[9]; Quentin Welniarz, PhD[1]; Marie Vidailhet, MD, PhD[1, 2]; Stephane Lehericy, MD, PhD[1, 2]; Sabine Meunier, MD, PhD[1]; Cecile Gallea, PhD[1]; Emmanuel Roze, MD, PhD[1, 2]

Equal Author Contributions:

Cecile Gallea and Emmanuel Roze are co-senior authors. These authors contributed equally to this work.

Corresponding Author:

Cecile Gallea

cecile.gallea.icm@gmail.com

Affiliation Information for All Authors: 1. Sorbonne Université, INSERM, CNRS, Paris Brain Institute, Paris, France 2. APHP Hôpital de La Pitié Salpêtrière, Assistance Publique des Hôpitaux de Paris, Sorbonne Université, Paris, France 3. Center for Magnetic Resonance Research, University of Minnesota, Minneapolis, USA 4. University of Nantes, CHU Nantes, CIC 1314, Nantes, France 5. Hôpital Robert-Debré, Paris, France 6. INM, Université de Montpellier, INSERM, CHU Montpellier, Département de Neuropédiatrie, Montpellier, France 7. Integrative and Cognitive Neurosciences Research (Unit EA481), Centre de génétique humaine, Université de Franche-Comté, Besançon, France 8. Univ. Lille, Inserm, CHU Lille, U1172 - LilNCog - Lille Neuroscience & Cognition, F-59000 Lille, France 9. Service de Génétique Moléculaire, Hôpital Saint-Louis, Assistance Publique des Hôpitaux de Paris, France.

Contributions:

Asya Ekmen: Drafting/revision of the manuscript for content, including medical writing for content; Major role in the acquisition of data; Analysis or interpretation of data

Aurelie Meneret: Drafting/revision of the manuscript for content, including medical writing for content; Major role in the acquisition of data

Romain Valabregue: Drafting/revision of the manuscript for content, including medical writing for content; Analysis or interpretation of data

Benoit Beranger: Study concept or design; Analysis or interpretation of data

Yulia Worbe: Drafting/revision of the manuscript for content, including medical writing for content; Analysis or interpretation of data

Jean-Charles Lamy: Drafting/revision of the manuscript for content, including medical writing for content; Major

role in the acquisition of data

Sofien Mehdi: Drafting/revision of the manuscript for content, including medical writing for content; Major role in the acquisition of data

Anais Herve: Drafting/revision of the manuscript for content, including medical writing for content; Major role in the acquisition of data

Isaac Adanyeguh: Drafting/revision of the manuscript for content, including medical writing for content; Analysis or interpretation of data

Gizem Temiz: Drafting/revision of the manuscript for content, including medical writing for content; Analysis or interpretation of data

Philippe Damier: Drafting/revision of the manuscript for content, including medical writing for content; Major role in the acquisition of data

Domitille Gras: Drafting/revision of the manuscript for content, including medical writing for content; Major role in the acquisition of data

Agathe Roubertie: Drafting/revision of the manuscript for content, including medical writing for content; Major role in the acquisition of data

Juliette Piard: Drafting/revision of the manuscript for content, including medical writing for content; Major role in the acquisition of data

Vincent Navarro: Drafting/revision of the manuscript for content, including medical writing for content; Major role in the acquisition of data

Eugenie Mutez: Drafting/revision of the manuscript for content, including medical writing for content; Major role in the acquisition of data

Florence Riant: Drafting/revision of the manuscript for content, including medical writing for content; Major role in the acquisition of data

Quentin Welniarz: Drafting/revision of the manuscript for content, including medical writing for content; Analysis or interpretation of data

Marie Vidailhet: Drafting/revision of the manuscript for content, including medical writing for content; Study concept or design; Analysis or interpretation of data

Stephane Lehericy: Drafting/revision of the manuscript for content, including medical writing for content; Study concept or design; Analysis or interpretation of data

Sabine Meunier: Drafting/revision of the manuscript for content, including medical writing for content; Study concept or design; Analysis or interpretation of data

Cecile Gallea: Drafting/revision of the manuscript for content, including medical writing for content; Major role in the acquisition of data; Study concept or design; Analysis or interpretation of data; Additional contributions: Cecile Gallea and Emmanuel Roze are co-senior authors. These authors contributed equally to this work.

Emmanuel Roze: Drafting/revision of the manuscript for content, including medical writing for content; Major role in the acquisition of data; Study concept or design; Analysis or interpretation of data

Number of characters in title: 75

Abstract Word count: 349

Word count of main text: 4478

References: 50

Figures: 5

Tables: 2

Clinical Trial registration number: NCT03481491

Supplemental: Supplemental Material STROBE checklist

Statistical Analysis performed by: Benoît Béranger, Paris Brain Institute - Sorbonne Univsersites, BSc Romain Valabregue, INSERM - Sorbonne Univsersites, PhD

Search Terms: [312] Cerebellum, [162] Dystonia, [313] Basal ganglia, [311] Motor cortex

Acknowledgements: The authors thank the patients, their families and their doctors for their participation and help. We also thank the Center for Clinical Investigations (CIC, Pitié Neurosciences 1422, Hôpital de la Pitié-Salpêtrière, Paris, France) and the platform TMS and CENIR (Institut du Cerveau, Paris, France) for their invaluable support with the acquisitions. We thank Isabelle Dusart for her precious scientific advice that was helpful in writing the manuscript. Wed like to thank Felicity Neilson for her language editing services. This work received financial support from « Association des malades atteints de dystonie (AMADYS) » and from « Fondation pour la Recherche Médicale (FRM) » (prix Line-Pomaret, grant attributed to A.E.). This project was also supported by « Agence Nationale de la Recherche (ANR) » under the frame of the European Joint Programme on Rare Diseases (EJP RD, ANR-16-CE37-0003-03). In addition, this project received funding from the European Union's Horizon 2020 research and innovation programme under the EJP RD COFUND-EJP N° 825575 - EurDyscover.

Study Funding: List of grants received for the present study: - « Association des malades atteints de dystonie (AMADYS) » - « Fondation pour la Recherche Médicale (FRM) » (prix Line-Pomaret, grant attributed to A.E.). - « Agence Nationale de la Recherche (ANR) » under the frame of the European Joint Programme on Rare Diseases (EJP RD, ANR-16-CE37-0003-03). - European Union's Horizon 2020 research and innovation programme under the EJP RD COFUND-EJP N° 825575 - EurDyscover.

Disclosures: None of the authors report any disclosures relevant to the manuscript.

Abstract

Background and Objectives: The main culprit gene for paroxysmal kinesigenic dyskinesia, characterized by brief and recurrent attacks of involuntary movements, is *PRRT2*. The location of the primary dysfunction associated with paroxysmal dyskinesia remains a matter of debate and may vary depending on the etiology. While striatal dysfunction has often been implicated in these patients, evidence from preclinical models indicate that the cerebellum could also play a role. We aimed to investigate the role of the cerebellum in the pathogenesis of PRRT2-related dyskinesia in humans.

Methods: We enrolled 22 consecutive right-handed patients with paroxysmal kinesigenic dyskinesia with a pathogenic variant of *PRRT2*, and their matched controls. Participants underwent a multi-modal neuroimaging protocol. We recorded anatomic and diffusion-weighted MRI, as well as resting-state functional MRI during which we tested the after-effects of sham and repetitive transcranial magnetic stimulation applied to the cerebellum on endogenous brain activity. We quantified: (i) the structural integrity of gray matter using voxel-based morphometry; (ii) the structural integrity of white matter using fixel-based analysis; (iii) the strength and direction of functional cerebellar connections using spectral dynamic causal modeling.

Results: *PRRT2* patients had: (i) decreased gray matter volume in the cerebellar lobule VI and in the medial prefrontal cortex; (ii) microstructural alterations of white matter in the cerebellum and along the tracts connecting the cerebellum to the striatum and the cortical motor areas; (iii) dysfunction of cerebellar motor pathways to the striatum and the cortical motor areas, as well as abnormal communication between the associative cerebellum (Crus I) and the medial prefrontal cortex. Cerebellar stimulation modulated communication within the

motor and associative cerebellar networks, and tended to restore this communication to the level observed in healthy controls.

Discussion: Patients with *PRRT2*-related dyskinesia have converging structural alterations of the motor cerebellum and related pathways with a dysfunction of cerebellar output towards the cerebello-thalamo-striato-cortical network. We hypothesize that abnormal cerebellar output is the primary dysfunction in patients with a *PRRT2* pathogenic variant, resulting in striatal dysregulation and paroxysmal dyskinesia. More broadly, striatal dysfunction in paroxysmal dyskinesia might be secondary to aberrant cerebellar output transmitted by thalamic relays in certain disorders.

Clinical trial number: NCT03481491 (https://ichgcp.net/clinical-trials-registry/NCT03481491)

Keywords: Paroxysmal Kinesigenic Dyskinesia; Cerebellum; Striatum; Motor Cortex; Connectivity.

Introduction

Paroxysmal kinesigenic dyskinesia (PKD) is characterized by brief and recurrent attacks of dystonia or other involuntary movements, typically triggered by sudden voluntary movements.[1] Monoallelic mutations of the *PRRT2* gene (HGNC:30500) account for up to 90% of familial cases of PKD and half of the sporadic cases depending on the population.[2,3]

The location of the primary dysfunction resulting in paroxysmal dyskinesia remains a question of debate and may vary depending on the etiology. The respective roles of the striatum and the cerebellum in its pathogenesis are likely critical.[4] For example, paroxysmal dyskinesia associated with GTP cyclohydrolase I deficiency is probably caused by the reduction in dopamine levels in the striatal microcircuitry[5], and lesions of the GPi, the main output of the basal ganglia receiving input from striatal projection neurons, can also result in paroxysmal dyskinesia.[6] Likewise, bilateral pallidal stimulation can improve paroxysmal dyskinesia in some patients.[7,8] Conversely, converging preclinical evidence indicates that cerebellar dysfunction plays a key role in paroxysmal dyskinesia associated with *ATP1A3* mutations.[9–11]

Patients with *PRRT2* monoallelic mutations rarely display episodic ataxia [3,12,13] whereas patients with biallelic mutations can have cerebellar atrophy and often experience prolonged episodes of cerebellar ataxia.[14,15] In keeping with these observations, the highest levels of *PRRT2* expression have been found in the cerebellar granule cells.[16,17] Specific suppression of *PRRT2* in these granule cells was sufficient to induce dyskinesia in mice.[18] While previous neuroimaging studies in patients with PKD have found anatomic or functional abnormalities in the basal ganglia, the thalamus and motor cortical regions, as well as the prefrontal cortex, the cerebellum is yet to be investigated.[19,20]

Here, we investigated the possibility that cerebellar dysfunction plays a critical role in the pathogenesis of *PRRT2*-related PKD. To this end, we combined a comprehensive anatomic and functional neuroimaging approach and transcranial magnetic stimulations of the cerebellum in a cohort of 22 patients with *PRRT2*-related PKD and 22 matched healthy controls.

Methods

Population

We enrolled 22 consecutive right-handed PKD patients with a pathogenic variant of *PRRT2*, and 22 healthy controls (HC) matched for age and gender. We collected the patients' history, demographic, genetic and clinical information. Patients with active epilepsy or a history of stroke were excluded. HCs were recruited from the database of the Pitié-Salpetrière Clinical Investigation Center (Paris, France). The patients were recruited through the French dystonia network.

Standard Protocol Approvals, Registrations, and Patient Consents

Prior to data collection, the full protocol was approved by the Regional Ethics Committee "Comité de Protection des Personnes Sud-Méditerranée" (reference: 17.060), and was registered on clinicaltrial.gov (NCT03481491). In accordance with the Declaration of Helsinki, written informed consent was obtained from all participants (or guardians of participants) in the study (consent for research).

Organization of the protocol

Both the HCs and patients were investigated during two visits on two consecutive days: the first was an anatomical MRI session; and the second a resting-state functional MRI (rsfMRI) session interleaved with cerebellar TMS (continuous theta burst stimulation, cTBS). Baseline rsfMRI data was first acquired before applying sham cerebellar TMS immediately followed by post-SHAM rsfMRI acquisition. After a pause of 30 minutes the patients underwent real cerebellar TMS immediately followed by post-cTBS fMRI acquisition. Between the cerebellar stimulations and MRI recordings, the participants were moved from the neighboring stimulation room to the MRI room on a non-magnetic wheelchair to minimize muscular activity.

Data acquisition

Patients treated for PKD with antiepileptics (n = 11) discontinued their treatment at least 1 week prior to the MRI session. MRI images were acquired using a 3T Siemens PRISMA system (Siemens, Erlangen, Germany) with a 32-channel head-neck coil

at the CENIR-ICM.

Anatomic MRI

During the first visit, we acquired a three-dimensional T1-weighted image (MP-RAGE) with the following characteristics: voxel size = 1 x 1 x 1 mm^3, field of view = 256 x 256 x 176 mm^3, repetition time = 6.172s, echo time = 3ms, flip angle = 90°. We also acquired diffusion-weighted images (EPI 2D) with the following characteristics: spatial resolution = 1.7 x 1.7 x 1.7 mm^3, b-factor = 2000, 1000, 300s/mm^2, gradient directions = 60, 32, 8, dimensions = 118 x 118 x 81 mm^3, EPI-factor = 128, repetition time = 3.5s, echo time = 75ms, flip angle = 90°.

The gradient directions were interleaved with four non-diffusion-weighted reference images (b0 images, b value = 0 s/mm^2). Another b0 image with an opposite phase-encoding blip was acquired to correct image distortions due to individual susceptibilities.

Functional MRI

During the second visit, we acquired functional resting-state images using a 9-min multi-echo multi-band echo-planar imaging (EPI) pulse sequence (2.5 mm isotropic resolution, 54 slices, TR/TE = 1600/15.2, 37.17, 59.14ms, multiband = 3, iPAT = 2, flip angle = 73°, field of view = 84 × 84 mm^2, pixel bandwidth = 2125 Hz). The participants were instructed to close their eyes and remain still during the scan and not to fall asleep. Their heart and respiratory rates were recorded by a digital sensor and a belt, and were used later to remove physiological noise from the BOLD signal. Each participant underwent three resting-state acquisitions (baseline, post-SHAM, post-cTBS).

Transcranial Magnetic Stimulation

During the second visit the participants were moved to the adjoining TMS room immediately after the baseline recordings. The intensity of the cerebellum stimulation was set according to the motor threshold (MT) for the right first dorsal interosseous (FDI) muscle[21]. To calculate the MT_{FDI}, the TMS pulses were applied over the left motor cortex with a 70-mm figure-of-eight coil connected to a magnetic stimulator (The Magstim Company Ltd, Whitland, UK). For repetitive TMS, the cerebellar lobule VIII was targeted with a neuronavigation system. The TMS coil was placed according to standard procedures (eAppendix 1) and maintained over this target during the 40-s stimulation period. A 70-mm figure-of-eight cooled coil connected to a SuperRapid^2 magnetic stimulator (The Magstim Company Ltd, Whitland, UK) was used to deliver the repetitive stimulation to the right cerebellum (ipsilateral to the dominant hand). The sham cerebellar stimulation applied after baseline recordings consisted

of 600 stimuli delivered at 10% of the MT in 3-pulse bursts at 50Hz repeated every 200ms.[22] Such stimulation does not modulate the cerebellar output.[23] After the 30-min pause that followed the post-SHAM resting-state acquisition, the participants were moved back to the stimulation room for cTBS, consisting of 600 stimuli delivered at 85% of the MT in 3-pulse bursts at 50Hz repeated every 200ms.[22] Such stimulation can modulate the cerebellar output for at least 30min.[23] The stimulation intensities were in accordance with the limit recommended by the current guidelines for delivering repeated TMS.[24] After having undergone all the TMS procedures, the participants were asked: "Which of the two TMS sessions did you think was the real stimulation?".

Data analysis

Population

Statistics were calculated using Matlab (MATLAB, *version 2017b*. Natick, Massachusetts: The MathWorks Inc.). Demographic parameters (age, gender and education level in total years of education starting from primary school) were compared between the groups using two sample t-tests. Answers to the TMS questionnaire were entered in a vector of 22 values for each group. Based on the fact that binary responses have a 50% chance of being randomly correct, we compared the 22 values of each group to a random vector composed of 1 and 0 values (matlab function "rand", 50% of 1 or 0 values) using a two-sample t-test.

Anatomic T1

We applied voxel-based morphometry (VBM) using the VBM8 toolbox (http://dbm.neuro.uni-jena.de/vbm) to compare regional gray matter differences between patients and HCs. Data preprocessing was performed following the standard VBM8 pipeline, with normalization of gray matter images in the Montreal Neurological Institute (MNI)

template space using Dartel. Non-linear modulation of normalized gray matter images was used to correct for individual brain sizes. Smoothing was applied with an 8-mm FWHM Gaussian kernel. All statistical designs included age, gender and total intracranial volume as nuisance regressors. We employed (1) a two-sample t-test to evaluate gray matter group differences; (2) a multiple regression analysis with disease duration and age at onset as covariables of interest to investigate the association of clinical parameters with gray matter maps. Results were thresholded at $P \leq 0.05$ using Probabilistic Threshold-free Cluster Enhancement (pTFCE) with family-wise error (FWE) correction across the whole brain.

Diffusion MRI

Using fixel-based analysis, we investigated white matter fiber density (FD, reflecting intra-axonal volume) and fiber-bundle cross-section (FC, the area occupied by the axons).[25] The term "fixel" here refers to the image unit, similar to a "voxel" but containing information about individual fiber orientation. Motion, bias field correction and global intensity normalization of the diffusion-weighted images were individually performed (see eAppendix 1). Fiber orientation distributions (FOD) were computed using constrained spherical deconvolution. The FODs were then used to create a study template to register all the individual FOD images into a common space. FD was estimated by non-parametric numerical integration using a dense sampling of the FOD. In addition, we estimated a fixel-specific measure based on morphology differences in the plane perpendicular to the fixel direction, and compared this measure across subjects to investigate variations in local FC. We compared measures of FD and FC in all white matter fixels across both groups using a General Linear Model, including age, gender and total intracranial volume as nuisance covariates. Connectivity-based smoothing and statistical inference were performed with Connectivity-based fixel enhancement using 2 million streamlines and default parameters (smoothing = 10-mm FWHM, C=0.5, E=2, H=3). FWE corrected p-values were assigned to

each fixel using non-parametric permutation testing with 5000 permutations. To better assess all the fiber pathways affected, we reconstructed the pathways that passed through regions of local structural alterations based on the whole-brain template-derived tractogram.

Functional MRI

Definition of Regions of Interest

Following pre-processing to combine the multiple echos, denoise and normalize the data to the MNI template space, we conducted an Independent Component Analysis (ICA) at the level of the group to identify regions of interest (ROIs) (GIFT software, version 3.0[26]) using 20 components (eAppendix 1). The cerebello-thalamo-striatal (CTS) loop comprised the cerebellum (cerebellar lobule VI and VIII, separately), the central medial nuclei of the thalamus (CM), and the sensorimotor striatum (posterior dorsal putamen). The cerebello-thalamo-motor cortex (CTM) loop comprises the cerebellum, the ventral intermediate nuclei of the thalamus (VIM), the primary sensorimotor cortex (SM1) and the supplementary motor area (SMA). Since functional abnormalities have been previously observed in the thalamus and medial prefrontal cortex[19], we tested whether these abnormalities could be related to aberrant cerebellar influence. We looked at the cerebellar Crus I that is anatomically connected to the prefrontal cortex through the medial dorsal thalamic nucleus (MD)[27] which we labeled the cerebello-thalamo-prefrontal (CTP) loop. Lastly, we examined the Default Mode Network (DMN) comprising the posterior cingulate cortex (PCC), the medial prefrontal cortex (mPFC) and the bilateral inferior parietal lobule (IPL).

Dynamic Causal Modeling

The spectral Dynamic Causal Modeling (DCM) analyses were conducted using DCM12 implemented in the SPM12 (revision 12.2). This method is more advantageous than conventional models: (i) to isolate group differences in connectivity parameters due to greater

consistency; and (ii) to evaluate connectivity differences across independent sessions.[28] DCM models were specified for each network (see eAppendix 1) as a fully connected model. Using spectral DCM[39], we obtained individual measures of causal interactions between regions, as well as the amplitude of endogenous neuronal fluctuations within each region.[30] We reported group and stimulation effects using the equivalent of a global linear model in the DCM framework[31] with age and gender as covariates of nuisance. We evaluated: (i) the average connectivity across subjects in each group; (ii) the between-group comparison (*PRRT2* vs HC); (iii) the between-session comparison for the *PRRT2* group (post-SHAM vs post-cTBS). We only report effects (i.e., changes in directed connectivity) that have a posterior probability >0.95, according to the Bayesian statistical framework.

Data availability

Anonymized data not published within this article will be made available on request from any qualified investigator if approved by the Internal Review Board. In their current status, the data are considered to be the intellectual property of the Paris Brain Institute and INSERM.

Results

Population

Patients' characteristics are summarized in Table 1. Twelve of the 22 HCs (55%) and 11 of the 22 patients (50%) gave the correct answer to the question about which one of the two sessions was the real stimulation. Neither group identified the sham from the real stimulation at a higher probability than chance (*PRRT2* patients: P=0.74; HCs: P=0.54).

Voxel-Based Morphometry

Gray matter volume (GMV) was lower in the bilateral cerebellar lobule VI and the right medial prefrontal cortex (mPFC) of the patients compared to the HCs **(Fig. 1A,** Table 2**)**. Reverse contrast failed to reveal any difference. Disease duration correlated with the bilateral cerebellum Crus II only: patients with longer disease duration had a lower GMV in Crus II (**eFig 1A-B**). Age at onset correlated with GMV in: i) the bilateral cerebellum Crus I and the left cerebellar lobule VI; and ii) the bilateral sensorimotor striatum: patients with an earlier age of onset of PKD had a lower GMV in these two areas (**Fig 1B-C**, **eFig 1C-D**).

Diffusion MRI

The patients had focal microstructural fiber abnormalities with changes in both within-voxel FD (**Fig. 2**) and FC (**eFig. 2**), which were both increased compared with the HCs. For FC, group differences were maximal in the motor lobule VI of the cerebellum and the mPFC. For FD, group differences were located at the proximal portion of the superior cerebellar peduncles, in the middle cerebellar peduncles as well as in the posterior limb of the internal capsule.

Structural alterations in the patients were located in areas intersecting the outgoing and incoming cerebellar pathways (Fig. 3). Many of the fiber pathways that connected to the affected cerebellar regions showed a significant increase in FD. Based on the anatomico-functional characteristics of these tracts, we identified outgoing fibers from the cerebello-thalamo-striato-cortical tract, incoming fibers from the cortico-cerebellar tract encompassing the middle cerebellar peduncle, and cortico-spinal tract encompassing the posterior regions of the internal capsule.

Functional MRI

Regions of interest

The CTM, CTS, CTP and DMN independent components were identified by the spatial ICA analysis (**eFig 3**). The spheres centered on the peaks (CTM, CTS, CTP) or on *a priori* coordinates (DMN) were used for further DCM analyses (**Fig. 4**; see coordinates in eAppendix 1).

Dynamic Causal Modeling

DCM group analysis showed that the patients had a dysfunction of cerebellar outputs within the CTS, CTM and CTP loops (**Fig. 5A**). Based on the mathematical sense, negative coupling parameters are associated with anti-correlated responses (inhibitory connections) between two nodes whereas positive coupling parameters are associated with correlated response (facilitatory connections) between two nodes.[29] For the CTS and CTM loops, the patients had decreased inhibition from the cerebellar lobule VIII to the thalamic relays. In contrast, the connection from the cerebellar lobule VI to the thalamic relays was less facilitated in the patients than in the HCs. Connections from the thalamic relays to the striatum (facilitated in patients and inhibited in HCs) and primary sensorimotor cortex (less inhibited in patients) were also disrupted. For the CTS, cerebellar dysfunction in the patients was accompanied by increased self-inhibition in the cerebellar lobule VI, cerebellar lobule VIII and the sensorimotor striatum. Self-inhibition was unchanged for cortical motor areas. In addition to the cerebellar and striatal dysfunctions of the motor circuits, we observed a difference in connectivity in the DMN, accompanied by a decrease in self-inhibition (self-facilitation) in the medial prefrontal cortex.

Continuous TBS modulation of the cerebellum tended to restore thalamo-cortical connectivity towards the level observed in the HCs: connections from the thalamic relays to the striatum and from the thalamic relays to the primary sensorimotor cortex were less

facilitated in the patients after cTBS (**Fig. 5B**). In the CTS, cTBS decreased self-inhibition of the cerebellar lobule VIII (target of the stimulation) and the sensorimotor striatum.

Discussion

For the first time, we show that patients with *PRRT2*-related PKD have converging structural alterations of the motor cerebellum and related pathways with a dysfunction of cerebellar output towards the cerebello-thalamo-striato-cortical network. Based on these findings and previous preclinical evidence, we suggest that abnormal cerebellar output is the primary dysfunction resulting in PKD in patients with a mutation of *PRRT2*. More broadly speaking, striatal dysfunction in paroxysmal dyskinesia might be secondary to aberrant cerebellar output transmitted to the striatum in certain disorders, such as in PRRT2-related PKD.

Strengths and limitations

The main strengths of our study lie in the homogeneity of the patient group (comprised exclusively of patients diagnosed with PKD with a pathogenic variant in *PRRT2)*, and the use of a cutting-edge multimodal imaging approach. Furthermore, our study was original in that we focused on cerebellar dysfunction, a concept supported by several very recent preclinical experiments.[16–18,32] However, a few limitations deserve to be mentioned. Firstly, some of our PKD patients were on chronic treatment, mainly comprising low dose carbamazepine. Hence, although highly unlikely, we cannot formally rule out that the chronic treatment had an influence on our structural findings. In addition, all PKD patients included in the study had the same c.649dupC pathogenic variant of the *PRRT2* gene, a variant which is implicated in around 75% of PRRT2-PKD patients and which leads to a premature stop codon. Nevertheless, it is thought that all the variants of this gene linked to PKD result in similar gene haploinsufficiency with a subsequent protein loss of function[33]. It is thus likely that the

effect of the mutation is representative of the PRRT2-PKD patient population and that this aspect does not interfere with the generalizability of our findings. Another potential limitation is that we did not randomize the order of the sham and active TMS sessions. This was because our protocol could not last more than two days, preventing us from measuring the effect of cerebellar TMS with a double-blind procedure and a sufficient wash-out period (typically 1 week). However, from the debriefing question, none of the patients (or HCs) who were naive to TMS could decipher the real from the sham stimulation.

Structural abnormalities of the motor cerebellum and cerebellar pathways in the *PRRT2*-PKD patients

Whole brain voxel-based analysis of the gray matter found a decrease in the (motor) lobule VI of the cerebellum. GMV in the cerebellar areas correlated with clinical characteristics. Patients with PKD onset at an early age had a lower GMV in the left cerebellar lobule VI and bilateral cerebellar Crus I. Patients with longer disease duration had a lower GMV in cerebellar Crus II. These results suggest a link between the cerebellum and the pathogenesis of the disease.

We found microstructural alterations in the patients located at the proximal portion of the superior cerebellar peduncles (conveying cerebellar efferents), in the middle cerebellar peduncles (conveying cerebellar afferents from the brain structures), as well as in the posterior limb of the internal capsule (conveying corticospinal tract fibers). Fixel-based analysis is a novel framework which provides fiber specific information to quantify white matter characteristics without anatomic *a priori*, unlike seed-to-target analysis. In our patients, the apparent FD was greater in the superior cerebellar peduncles, likely reflecting a larger number of axons in that fiber population or the presence of bigger axons.[25] In addition, FC was greater in the motor cerebellum (lobule VI) and the medial prefrontal cortex. This may account for an increase in the spatial extent occupied by the white matter fibers due to

abnormal axonal growth or an overexpansion of cerebellar outputs.[25] These changes in tissue microstructure can modify the capacity of the fiber bundle to relay information in the cerebellum. Moreover, microstructural alterations were found in posterior regions of the internal capsule. These tracts connect primary sensorimotor regions, as well as the parietal lobe to the spinal cord.[34] The contributions from the sensory areas terminate in the sensory nuclei of the brainstem and spinal cord (which are below the field of view of the diffusion-weighted imaging data), where they modulate sensory transmission. This might suggest that sensory information is processed differently in *PRRT2-PKD* patients compared to healthy subjects.

Three studies have investigated structural abnormalities in PKD patients using other techniques. Two of them used graph theory applied on structural covariance of GMV[35] and white matter properties[36] but did not include the cerebellum in the construction of the morphological network used in the analyses. The remaining study investigated the basal ganglia and found a decrease in GMV, and white matter abnormalities in the medial thalamus in PKD patients.[37] Furthermore, another study, using seed-to-target analyses, found increased structural connectivity in the thalamo-cortical motor tract in PKD patients.[38] Our results indicate that structural connectivity was also altered between the cerebellum and the thalamic relay, upstream of the thalamo-cortical tract.

Abnormal cerebellar functional output towards the thalamo-striato-cortical network

Using spectral DCM, we found a reduction in the information flow from the motor cerebellar lobule VI to the thalamic relay and an altered drive of the thalamic relay towards the striatum and the primary motor cortex (**Fig. 5C**), probably resulting in a modification of the balance between the striatal and the motor cortex activity. This finding is consistent with microstructural white matter abnormalities of the cerebellar outputs, indicating abnormal

axonal growth or an overexpansion of cerebellar outputs. A previous resting-state study of 11 PKD patients of unknown genetic cause found an increased interhemispheric functional connectivity in the basal ganglia-thalamo-cortical network and the cerebellum.[39] Similar changes in the connectivity pattern in the cerebello-thalamo-striato-cortical network have been modeled in dopa-induced dyskinesia of Parkinson's disease (PD).[40,41] Although PD dyskinesia and PKD constitute two different clinical and pathophysiological paradigms, they share similarities, namely episodic hyperkinetic movements associated with striatal dysfunction. Of note, in our *PRRT2-PKD* patients, the thalamic drive was altered to a greater extent towards the striatum than towards the primary motor cortex. This highlights the importance of cerebello-striatal pathway dysfunction in explaining PKD pathophysiology.

In addition to the communication between nodes, our DCM approach investigated another class of connectivity parameters: self-inhibitory or intrinsic connections. Intrinsic connections reflect how sensitive a region is to afferent inputs. A reduction in intrinsic connections is thus a vector of internal instability. We observed a decrease in self-inhibition in cerebellar and striatal nodes in our *PRRT2-PKD* patients, suggesting internal instability of the motor cerebellum and motor striatum. TMS-induced modulation of cerebellar output tended to restore cerebellar self-inhibition and thalamo-striatal and thalamo-cortical motor connectivity. This fits with the fact that modulation of cerebellar drive can change corticostriatal plasticity[42] and can affect thalamo-cortical[23] or cortico-cortical coupling.[43] The type of stimulation we used induced a decrease of the inhibitory input of the cerebellar cortex onto the dentate. This would eventually lead to a facilitation of glutamatergic connections between the dentate and the thalamus, and between the thalamus and cortical motor areas.

Medial prefrontal cortex abnormalities in *PRRT2*-PKD patients

Our study provides further evidence of medial prefrontal cortex dysfunction in *PRRT2*-PKD patients. More specifically, we found an increase in self-inhibition in the prefrontal node, dysregulated connectivity from the thalamus to the prefrontal cortex, and a decrease in GMV of medial prefrontal areas. Previous studies have also found structural alterations of the medial prefrontal area.[19,38] In addition, our results show that medial prefrontal cortex connectivity is modified by an alteration of the cerebellar drive on thalamic relay, leading to an enhanced excitatory coupling between the thalamic relay and the medial prefrontal cortex. A study involving eight *PRRT2*-related PKD patients found decreased functional connectivity between the thalamus and the prefrontal cortex compared to non-mutated PKD patients and controls.[38] Furthermore, cerebellar TMS restored thalamo-prefrontal connectivity and impacted prefrontal cortex sensitivity to inputs (decrease in self-inhibition). This indicates that the cerebellum can influence prefrontal activity in *PRRT2*-related PKD patients. Reciprocal anatomic loops exist between the cerebellum and the medial prefrontal cerebral cortex.[44] The prefrontal cortex receives substantial input from thalamic regions including the zone of termination of cerebellar afferents.[45] In addition, we found that connectivity in the default brain network, including the medial prefrontal area, was also disrupted (Fig. 5A). This shows that dysfunction of the medial prefrontal cortex could be explained by, or be associated with, dysfunction of cerebral cortical nodes in addition to the cerebellum. Interestingly, modulation of prefrontal activity with repetitive TMS can influence functional connectivity between the medial prefrontal cortex and the striatum.[46] This suggests that dysfunction of the striatum and the medial prefrontal cortex could be linked in a positive loop gain as a Larsen effect (i.e., self-amplified activity). We think that the disorder of the prefrontal network might link the classic triggering factors of *PRRT2*-PKD and the role of this network in anticipating outcomes and shifting attention.[45]

From cerebellar dysfunction in PRRT2 patients to the pathogenesis of paroxysmal dyskinesia

Various preclinical evidence supports the role of the cerebellum in the pathogenesis of *PRRT2*-related PKD. The highest level of *PRRT2* expression is found in the cerebellum (granule cell and molecular layers) with the RNA transcript exclusively located within the granule cells of the cerebellar cortex.[16,17] Granule cells in *PRRT2* knockout mice had an increased intrinsic excitability with abnormal sodium currents.[32] *PRRT2*-KO recapitulating the human PKD phenotype had a higher excitatory strength of the synapses at the parallel fibers between granule cells and Purkinje cells during high frequency stimulation.[16] Specific suppression of *PRRT2* in the granule cells (but not the cortex or the striatum) in the mice was sufficient to bring about heat-induced dyskinesia associated with abnormal firing of the Purkinje cells.[18] Altogether, these experiments demonstrate abnormal excitability of the granule cells (expressing *PRRT2*) that induces synaptic dysfunction between the granule and Purkinje cells within the molecular layer.[16–18,32] This synaptic dysfunction likely results in a disruption of the normal inhibitory control of the Purkinje cells on deep cerebellar nuclei, which eventually transmit the final excitatory output from the cerebellum to the thalamus and related subcortical and cortical motor networks. Our findings together with data from animal models and human experiments provide converging evidence that the cerebellum is the primary location of the disorder and that subsequent dysfunction of the cerebello-thalamo-striatal network causes *PRRT2*-PKD.

Likewise, paroxysmal dystonic episodes linked to mutations in the *ATP1A3* gene are associated with altered cerebellar activity which is transmitted to the deep cerebellar nuclei.[9–11] Selective lesions of these nuclei or their thalamic relay, as well as drug-induced cerebellar inhibition, can alleviate dystonic episodes in animal models of the disease. Tottering Mice have dystonic attacks associated with a maladaptive plasticity involving upregulation of

calcium channels in the cerebellum, and degeneration of the Purkinje cells stop the dystonic episodes in these mice.[47] Similarly, removal of the cerebellum eliminates paroxysmal episodes in lethargic mice carrying a mutation in the calcium channel beta subunit 4 (*CCHB4*) gene.[48] Rodent and non-human primates have a di-synaptic pathway linking cerebellar nuclei to the striatum that is critical for motor control.[42,49,50] We hypothesize that paroxysmal dystonia/dyskinesia is a network disorder mainly characterized by striatal dysfunction that could be either primary or secondary to aberrant cerebellar output transmitted to the striatum, as in *PRRT2*- or ATP1A3-related paroxysmal dyskinesia. Cerebellar dysfunction could also influence the final motor output without incorporating the striatum, especially through the cerebellar projection on the various motor areas after a thalamic relay, the motor areas being the main origin of the corticospinal tract.

Acknowledgements

The authors thank the patients, their families and their doctors for their participation and help. We also thank the Center for Clinical Investigations (CIC, Pitié Neurosciences 1422, Hôpital de la Pitié-Salpêtrière, Paris, France) and the platform TMS and CENIR (Institut du Cerveau, Paris, France) for their invaluable support with the acquisitions. We thank Isabelle Dusart for her precious scientific advice that was helpful in writing the manuscript. We'd like to thank Felicity Neilson for her language editing services. This work received financial support from « Association des malades atteints de dystonie (AMADYS) » and from « Fondation pour la Recherche Médicale (FRM) » (prix Line-Pomaret, grant attributed to A.E.). This project was also supported by « Agence Nationale de la Recherche (ANR) » under the frame of the European Joint Programme on Rare Diseases (EJP RD, ANR-16-CE37-0003-03). In addition, this project received funding from the European Union's Horizon 2020 research and innovation programme under the EJP RD COFUND-EJP N° 825575 - EurDyscover.

Competing interests

The authors report no competing interests.

Supplementary material

Supplementary material is available in eAppendix 1 at *Neurology* online in a separate file.

References

1. Méneret A, Roze E. Paroxysmal movement disorders: An update. *Rev Neurol (Paris)*. 2016;172(8-9):433-445. doi:10.1016/j.neurol.2016.07.005

2. Chen W-J, Lin Y, Xiong Z-Q, et al. Exome sequencing identifies truncating mutations in PRRT2 that cause paroxysmal kinesigenic dyskinesia. *Nat Genet*. 2011;43(12):1252-1255. doi:10.1038/ng.1008

3. Meneret A, Grabli D, Depienne C, et al. PRRT2 mutations: A major cause of paroxysmal kinesigenic dyskinesia in the European population. *Neurology*. 2012;79(2):170-174. doi:10.1212/WNL.0b013e31825f06c3

4. Delorme C, Giron C, Bendetowicz D, Méneret A, Mariani LL, Roze E. Current challenges in the pathophysiology, diagnosis, and treatment of paroxysmal movement disorders. *Expert Rev Neurother*. 2020;00(00):1-17. doi:10.1080/14737175.2021.1840978

5. Dale RC, Melchers A, Fung VSC, Grattan-Smith P, Houlden H, Earl J. Familial paroxysmal exercise-induced dystonia: atypical presentation of autosomal dominant GTP-cyclohydrolase 1 deficiency. *Dev Med Child Neurol*. 2010;52(6):583-586. doi:10.1111/j.1469-8749.2010.03619.x

6. Friedman J, Feigenbaum A, Chuang N, Silhavy J, Gleeson JG. Pyruvate dehydrogenase complex-E2 deficiency causes paroxysmal exercise-induced dyskinesia. *Neurology*. 2017;89(22):2297-2298. doi:10.1212/WNL.0000000000004689

7. de Almeida Marcelino AL, Mainka T, Krause P, Poewe W, Ganos C, Kühn AA. Deep brain stimulation reduces (nocturnal) dyskinetic exacerbations in patients with ADCY5 mutation: a case series. *J Neurol*. 2020;267(12):3624-3631. doi:10.1007/s00415-020-09871-8

8. van Coller R, Slabbert P, Vaidyanathan J, Schutte C. Successful treatment of disabling paroxysmal nonkinesigenic dyskinesia with deep brain stimulation of the globus

pallidus internus. *Stereotact Funct Neurosurg*. 2014;92(6):388-392. doi:10.1159/000365226

9. Calderon DP, Fremont R, Kraenzlin F, Khodakhah K. The neural substrates of rapid-onset Dystonia-Parkinsonism. *Nat Neurosci*. 2011;14(3):357-365. doi:10.1038/nn.2753

10. Fremont R, Calderon DP, Maleki S, Khodakhah K. Abnormal high-frequency burst firing of cerebellar neurons in rapid-onset dystonia-parkinsonism. *J Neurosci Off J Soc Neurosci*. 2014;34(35):11723-11732. doi:10.1523/JNEUROSCI.1409-14.2014

11. Fremont R, Tewari A, Khodakhah K. Aberrant Purkinje cell activity is the cause of dystonia in a shRNA-based mouse model of Rapid Onset Dystonia-Parkinsonism. *Neurobiol Dis*. 2015;82:200-212. doi:10.1016/j.nbd.2015.06.004

12. Gardiner AR, Bhatia KP, Stamelou M, et al. PRRT2 gene mutations: From paroxysmal dyskinesia to episodic ataxia and hemiplegic migraine. *Neurology*. 2012;79(21):2115-2121. doi:10.1212/WNL.0b013e3182752c5a

13. Legris N, Chassin O, Nasser G, Riant F, Tournier-Lasserve E, Denier C. Acute-Onset Ataxia and Transient Cerebellar Diffusion Restriction Associated with a PRRT2 Mutation. *J Stroke Cerebrovasc Dis*. 2019;28(2):e3-e4. doi:10.1016/j.jstrokecerebrovasdis.2018.10.021

14. Labate A, Tarantino P, Viri M, et al. Homozygous c.649dupC mutation in PRRT2 worsens the BFIS/PKD phenotype with mental retardation, episodic ataxia, and absences. *Epilepsia*. 2012;53(12):e196-199. doi:10.1111/epi.12009

15. Delcourt M, Riant F, Mancini J, et al. Severe phenotypic spectrum of biallelic mutations in *PRRT2* gene. *J Neurol Neurosurg Psychiatry*. 2015;86(7):782-785. doi:10.1136/jnnp-2014-309025

16. Michetti C, Castroflorio E, Marchionni I, et al. The PRRT2 knockout mouse recapitulates the neurological diseases associated with PRRT2 mutations. *Neurobiol Dis*. 2017;99. doi:10.1016/j.nbd.2016.12.018

17. Calame DJ, Xiao J, Khan MM, et al. Presynaptic PRRT2 Deficiency Causes Cerebellar Dysfunction and Paroxysmal Kinesigenic Dyskinesia. *Neuroscience*. 2020;448:272-286. doi:10.1016/j.neuroscience.2020.08.034

18. Tan G-H, Liu Y-Y, Wang L, et al. PRRT2 deficiency induces paroxysmal kinesigenic dyskinesia by regulating synaptic transmission in cerebellum. *Cell Res*. 2018;28(1):90-110. doi:10.1038/cr.2017.128

19. Liu W, Xiao Y, Zheng T, Chen G. Neural Mechanisms of Paroxysmal Kinesigenic Dyskinesia: Insights from Neuroimaging. *J Neuroimaging*. Published online 2020:1-5. doi:10.1111/jon.12811

20. Zhang Y, Ren J, Qin Y, et al. Altered topological organization of functional brain networks in drug-naive patients with paroxysmal kinesigenic dyskinesia. *J Neurol Sci*. 2020;411:116702. doi:10.1016/j.jns.2020.116702

21. Rossini PM, Barker AT, Berardelli A, et al. Non-invasive electrical and magnetic stimulation of the brain, spinal cord and roots: basic principles and procedures for routine clinical application. Report of an IFCN committee. *Electroencephalogr Clin Neurophysiol*. 1994;91(2):79-92. doi:10.1016/0013-4694(94)90029-9

22. Huang Y-Z, Edwards MJ, Rounis E, Bhatia KP, Rothwell JC. Theta burst stimulation of the human motor cortex. *Neuron*. 2005;45(2):201-206. doi:10.1016/j.neuron.2004.12.033

23. Popa T, Russo M, Meunier S. Long-lasting inhibition of cerebellar output. *Brain Stimulat*. 2010;3(3):161-169. doi:10.1016/j.brs.2009.10.001

24. Rossi S, Hallett M, Rossini PM, Pascual-Leone A. Safety, ethical considerations, and application guidelines for the use of transcranial magnetic stimulation in clinical practice and research. *Clin Neurophysiol*. 2012;120(12):323-330. doi:10.1016/j.clinph.2009.08.016.Rossi

25. Raffelt DA, Tournier J-D, Smith RE, et al. Investigating white matter fibre density and morphology using fixel-based analysis. *NeuroImage*. 2017;144(Pt A):58-73. doi:10.1016/j.neuroimage.2016.09.029

26. Calhoun VD, Adali T, Stevens MC, Kiehl KA, Pekar JJ. Semi-blind ICA of fMRI: A method for utilizing hypothesis-derived time courses in a spatial ICA analysis. *NeuroImage*. 2005;25(2):527-538. doi:10.1016/j.neuroimage.2004.12.012

27. Coffman KA, Dum RP, Strick PL. Cerebellar vermis is a target of projections from the motor areas in the cerebral cortex. *Proc Natl Acad Sci*. 2011;108(38):16068-16073. doi:10.1073/pnas.1107904108

28. Park H-J, Friston KJ, Pae C, Park B, Razi A. Dynamic effective connectivity in resting state fMRI. *NeuroImage*. 2018;180:594-608. doi:10.1016/j.neuroimage.2017.11.033

29. Friston KJ, Kahan J, Biswal B, Razi A. A DCM for resting state fMRI. *NeuroImage*. 2014;94:396-407. doi:10.1016/j.neuroimage.2013.12.009

30. Razi A, Kahan J, Rees G, Friston KJ. Construct validation of a DCM for resting state fMRI. *NeuroImage*. 2015;106:1-14. doi:10.1016/j.neuroimage.2014.11.027

31. Friston KJ, Litvak V, Oswal A, et al. Bayesian model reduction and empirical Bayes for group (DCM) studies. *NeuroImage*. 2016;128:413-431. doi:10.1016/j.neuroimage.2015.11.015

32. Binda F, Valente P, Marte A, Baldelli P, Benfenati F. Increased responsiveness at the cerebellar input stage in the PRRT2 knockout model of paroxysmal kinesigenic dyskinesia. *Neurobiol Dis*. 2021;152:105275. doi:10.1016/j.nbd.2021.105275

33. Landolfi A, Barone P, Erro R. The Spectrum of PRRT2-Associated Disorders: Update on Clinical Features and Pathophysiology. *Front Neurol*. 2021;12:629747. doi:10.3389/fneur.2021.629747

34. Rizzolatti G, Luppino G. The Cortical Motor System. *Neuron*. 2001;31(6):889-901. doi:10.1016/S0896-6273(01)00423-8

35. Li X, Lei D, Niu R, et al. Disruption of gray matter morphological networks in patients with paroxysmal kinesigenic dyskinesia. *Hum Brain Mapp*. 2020;42(2):398-411. doi:10.1002/hbm.25230

36. Li L, Lei D, Suo X, et al. Brain structural connectome in relation to PRRT2 mutations in paroxysmal kinesigenic dyskinesia. *Hum Brain Mapp*. 2020;41(14):3855-3866. doi:10.1002/hbm.25091

37. Kim JH, Kim DW, Kim JB, Suh S il, Koh SB. Thalamic involvement in paroxysmal kinesigenic dyskinesia: A combined structural and diffusion tensor MRI analysis. *Hum Brain Mapp*. 2015;36(4):1429-1441. doi:10.1002/hbm.22713

38. Long Z, Xu Q, Miao H-H, et al. Thalamocortical dysconnectivity in paroxysmal kinesigenic dyskinesia: Combining functional magnetic resonance imaging and diffusion tensor imaging: Thalamocortical Dysconnectivity In PKD. *Mov Disord*. 2017;32(4):592-600. doi:10.1002/mds.26905

39. Ren J, Lei D, Yang T, et al. Increased interhemispheric resting-state functional connectivity in paroxysmal kinesigenic dyskinesia: a resting-state fMRI study. *J Neurol Sci*. 2015;351(1-2):93-98. doi:10.1016/j.jns.2015.02.046

40. Caligiore D, Pezzulo G, Baldassarre G, et al. Consensus Paper: Towards a Systems-Level View of Cerebellar Function: the Interplay Between Cerebellum, Basal Ganglia, and Cortex. *The Cerebellum*. 2017;16(1):203-229. doi:10.1007/s12311-016-0763-3

41. Kishore A, Popa T. Cerebellum in Levodopa-Induced Dyskinesias: The Unusual Suspect in the Motor Network. *Front Neurol*. 2014;5:157. doi:10.3389/fneur.2014.00157

42. Chen CH, Fremont R, Arteaga-Bracho EE, Khodakhah K. Short latency cerebellar modulation of the basal ganglia. *Nat Neurosci*. 2014;17(12):1767-1775. doi:10.1038/nn.3868

43. Popa D, Spolidoro M, Proville RD, Guyon N, Belliveau L, Léna C. Functional role of the cerebellum in gamma-band synchronization of the sensory and motor cortices. *J Neurosci*. 2013;33(15):6552-6556. doi:10.1523/JNEUROSCI.5521-12.2013

44. Strick PL, Dum RP, Fiez JA. Cerebellum and nonmotor function. *Annu Rev Neurosci*. 2009;32:413-434. doi:10.1146/annurev.neuro.31.060407.125606

45. Middleton FA, Strick PL. Cerebellar projections to the prefrontal cortex of the primate. *J Neurosci Off J Soc Neurosci*. 2001;21(2):700-712. doi:10.1523/JNEUROSCI.21-02-00700.2001

46. Popa T, Morris LS, Hunt R, et al. Modulation of resting connectivity between the mesial frontal cortex and basal ganglia. *Front Neurol*. 2019;10:587. doi:10.3389/fneur.2019.00587

47. Campbell DB, North JB, Hess EJ. Tottering mouse motor dysfunction is abolished on the Purkinje cell degeneration (pcd) mutant background. *Exp Neurol*. 1999;160(1):268-278. doi:10.1006/exnr.1999.7171

48. Devanagondi R, Egami K, LeDoux MS, Hess EJ, Jinnah HA. Neuroanatomical substrates for paroxysmal dyskinesia in lethargic mice. *Neurobiol Dis*. 2007;27(3):249-257. doi:10.1016/j.nbd.2007.05.001

49. Hoshi E, Tremblay L, Féger J, Carras PL, Strick PL. The cerebellum communicates with the basal ganglia. *Nat Neurosci*. 2005;8(11):1491-1493. doi:10.1038/nn1544

50. Xiao L, Bornmann C, Hatstatt-Burklé L, Scheiffele P. Regulation of striatal cells and goal-directed behavior by cerebellar outputs. *Nat Commun*. 2018;9(1):3133. doi:10.1038/s41467-018-05565-y

Figure legends

Figure 1. Gray matter volumetric abnormalities in *PRRT2* patients. (**A**) Results of the two-sample t-test comparing gray matter volume (GMV) between *PRRT2*-PKD patients and healthy controls (HC). Main clusters showing a group difference are displayed on a 3D render; P <0.001 TFCE correction. (**B-C**) Results of the multiple regression analysis showing the GMV correlation with age at disease onset (P <0.001). The corresponding coordinates of peak changes are given in Table 2. mPFC: medial prefrontal cortex, CbVI: cerebellar lobule VI, SMPut: sensorimotor territory of putamen, SMCaud: caudate sensorimotor territory of caudate, VBM: voxel-based morphometry, SPM: statistical parametric mapping.

Figure 2. Fixel-based analysis comparing white matter structure in *PRRT2*-PKD patients and healthy controls. Fixels with a significant (P <0.05) increase in fiber density (FD) in patients compared to healthy controls. Yellow frames show the areas of interest with fixel abnormalities, which are enlarged on the right. The fixels that are displayed show significant group difference with family-wise error (FWE) corrected p-values and overlaid on the total voxel-wise group template. All significant differences are displayed by a black fixel. Fixel-based analysis enables fiber tract-specific inference by attributing p-values to each fixel

in voxels containing multiple fiber populations. (**A**) axial view of the cerebellum (left), enlarged at the level of the middle cerebellar peduncule (right). (**B**) axial view of the cerebellum, enlarged at the level of the superior cerebellar peduncle (right). (**C**) axial view of the cerebrum (left), enlarged at the level of the internal capsule (right). CbP: cerebellar peduncles.

Figure 3. Identification of white matter pathways carrying microstructural abnormalities in *PRRT2*-PKD patients on fixel-based analysis. The figure shows streamlines that pass through white matter fixels with a significant increase in fiber density comparing *PRRT2*-PKD patients and healthy controls (yellow frames in Figure 2). The tracts passing through these regions are superimposed on the sagittal (top left) and coronal (top right) views of the FD template. Multiple axial views are displayed to appreciate the trajectory of the tracts. These tracts were filtered from the whole brain tractography (red tracts are connecting the right brain hemisphere; blue tracts are connecting the left-brain hemisphere). **(A)** Cerebello-thalamo-striato-cortical tract passing through the superior cerebellar peduncles (outgoing cerebellar tract). The axial views are at the level of cerebellar dentate nucleus (a), superior cerebellar peduncles (b), midbrain (c), thalamus (d), striatum (e). **(B)** Cortico-ponto-cerebellar tract passing through the middle cerebellar peduncles (incoming cerebellar tract). The axial views are at the level of the striatum (a), the anterior bundle of the mesencephalon (b), the decussation of the cerebellar tract (c), the middle cerebellar peduncles (d), the cerebellar hemispheres (e). **(C)** Cortico-spinal tract passing through the internal capsule. The axial views are at the level of posterior part of the internal capsule (a), lateral part of the anterior bundle of the mesencephalon (b), the upper pons (c), the lower pons (d), the anterior bundle of the upper spinal cord (e). For each view (axial, coronal and sagittal), a

single 2D slice of fixels is shown and overlaid on the group template. CbP: cerebellar peduncles.

Figure 4. Regions of interest for resting-state connectivity defined from the independent component analysis. Regions of interest of the cerebellar loops and DMN defined as spheres from the components shown in eFigure 3. (**A**) Cortical motor areas: supplementary motor area (SMA), primary sensorimotor cortex (SM1). (**B**) Subcortical areas: sensorimotor territory of putamen (SM putamen), Ventral-Intermediate nucleus of the thalamus (VIM), Central-Medial nucleus of the thalamus (CM), Medial-Dorsal nucleus of the thalamus (MD). (**C**) Cerebellar areas: cerebellar lobule VI (Cb VI), cerebellar lobule VIII (Cb VIII), cerebellar CrusI (Cb CrusI). (**D**) Cortical areas of the default mode network: medial prefrontal cortex (mPFC); posterior cingulate cortex (PCC); left and right inferior parietal cortex (IPC).

Figure 5. Resting state connectivity estimates of the group analysis using spectral dynamic causal modeling. The cerebellar networks include cerebellar regions of the right hemisphere, and cerebral regions of the left hemisphere. **(A)** Results of the comparison between healthy controls (HC) and *PRRT2* patients at baseline. The networks of interest are displayed in lines, whereas within (HC, *PRRT2*) and between (HV ≠ *PRRT2*) group results are displayed in columns. (**B**) Results of the comparison between the session following cerebellar SHAM stimulation (SHAM) and the session following cerebellar real stimulation (cTBS) in *PRRT2* patients. The networks of interest are displayed in lines, whereas within (SHAM, cTBS) and between (SHAM ≠ cTBS) session results are displayed in columns. Posterior estimates for each connection (Exact values in eTable 2-5) are represented by

arrows (only for the posterior expectations of connections within 95% confidence intervals). Within group results represent the commonalities between the Bayesian parameter averages of each session (A for baseline, B for post-SHAM and post-cTBS). Self-connections (within region) are displayed with circular arrows, whereas the extrinsic (between regions) connections are displayed with straight arrows. Arrows are in red when positive or in blue when negative for within group results; in black in case of a significant difference, in gray in case of a non-significant difference for the group analyses. The thickness of the arrow is indicative of the connection strength. **(C)** Simplified schema of DCM extrinsic and self-connections that are different between groups (left) or modulated by cerebellar TMS in *PRRT2* patients (right); red for positive and blue for negative, only significant differences are displayed. cTBS : continuous theta burst stimulation; SMPut: putamen, sensorimotor territory; CM: central-medial nucleus of the thalamus; CbVI: Cerebellum lobule VI; Cb VIII: Cerebellum lobule VIII; SMA: supplementary motor area; SM1: primary sensorimotor cortex; VIM: ventral-intermediate nucleus of the thalamus; mPFC: medial prefrontal cortex; MD: medial-dorsal nucleus of the thalamus; Crus I: cerebellar Crus I; LIPC: left inferior parietal cortex; RIPC: right inferior parietal cortex; PCC: posterior cingulate cortex.

Tables

Table 1 Demographic and clinical characteristics of *PRRT2* patients and healthy controls. *PRRT2* patients and healthy controls did not differ in age, gender or educational level. Quantitative data are expressed as mean (±SD)

Characteristics	***PRRT2* Patients (n=22)**	**Healthy Controls (n=22)**	**P value**[a]
Age (years)	29.4 (± 12.2)	30.6 (± 11.7)	0.74
Age range (years)	15 – 49	19 – 54	
Gender (female/male)	8/14	8/14	
Education (total years from primary school)	14.0 (± 3.7)	15.4 (± 2.3)	0.12
Mutation (c.649dupC/other)	22/0		
Age at onset (years)	9.1 (± 3.2)		
Disease duration (years)	17.2 (± 10.6)		
Family history (yes/no)	18/4		

Dyskinesia type (dystonia/chorea/ballism)	22/0/0
Attack duration (<15s/<30s/60s)	7/9/6
Attack frequency (monthly)	15.0 (± 15.4)
Attack localization (focal/unilateral/bilateral)	1/1/20
Facial involvement (yes/no)	5/17
Treatment (yes/no)	11/11
Medication (CBZ/LTG/LEV[b])	8/2/1
Prognosis (good/bad)	22/0

[a]Two-tailed two-sample t test
[b]CBZ, carbamazepine; LTG, lamotrigine; LEV, levetiracetam; s, seconds

Table II Results of the group difference of gray matter volume (Voxel-Based Morphometry). MNI = Montreal Neurological Institute, AAL = automated anatomical labelling, HC = healthy controls, L = left, R = right, PFC = prefrontal cortex, ACC = anterior cingulate cortex.

Anatomic localization of clusters	**MNI coordinates of global maxima**	**Cluster size (number of voxels)**	**Statistics (z-score)**
(Reference = AAL atlas)	[x, y, z]		
HC > *PRRT2*			
L Cerebellum (lobule VI, dentate)	-15, -60, -26	350	3.65
R Medial PFC (superior frontal gyrus)	15, 66, 4	156	3.63
R ACC	8, 44, 24	145	3.49
R Cerebellum (lobule VI, dentate)	10, -60, -26	127	3.35

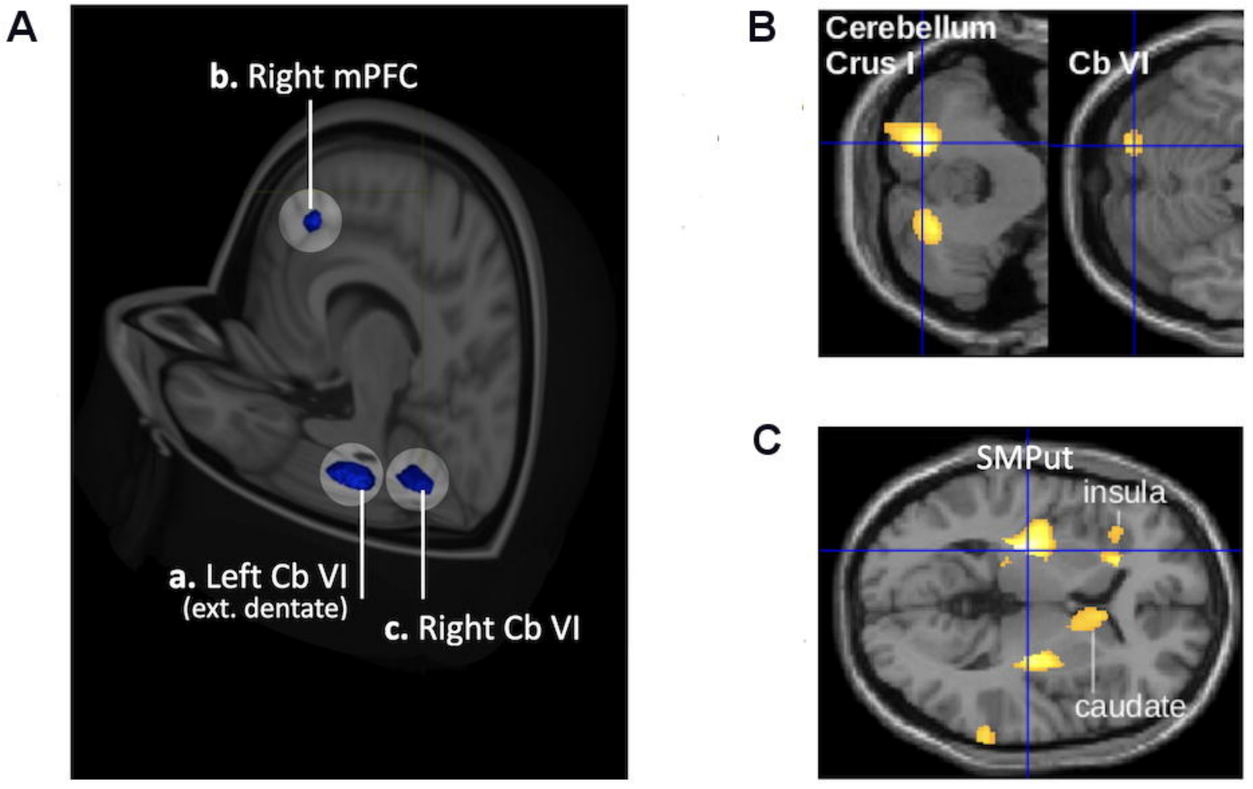
A
b. Right mPFC
a. Left Cb VI
(ext. dentate)
c. Right Cb VI
B
Cerebellum
Crus I
Cb VI
C
SMPut
insula
caudate

A

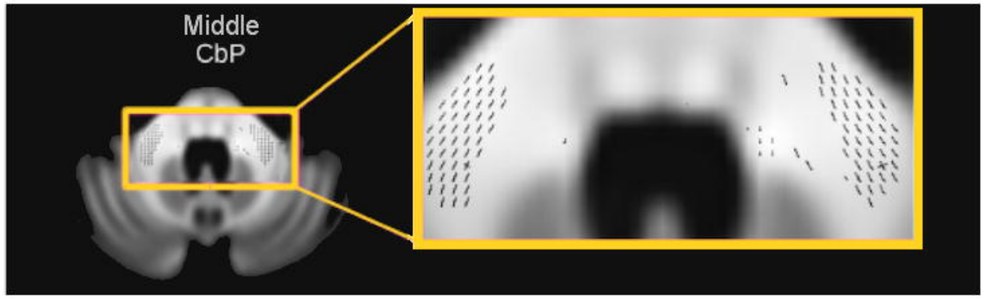

B

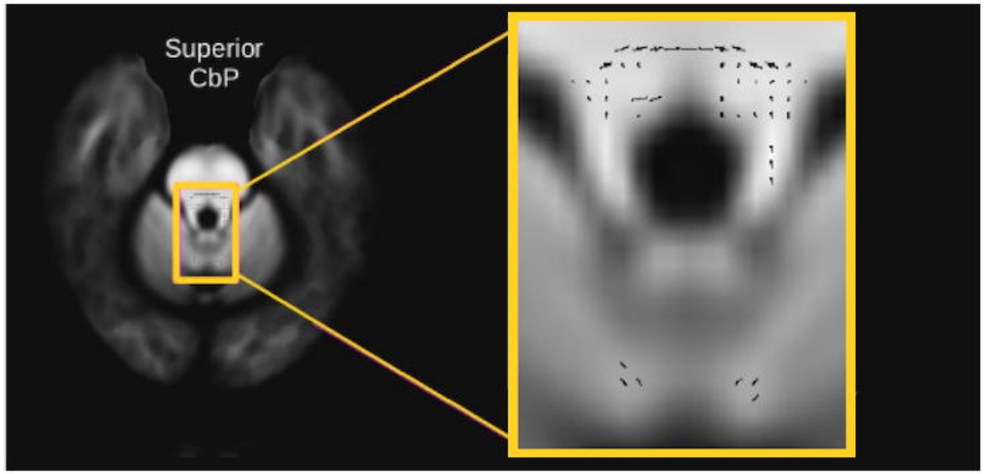

C

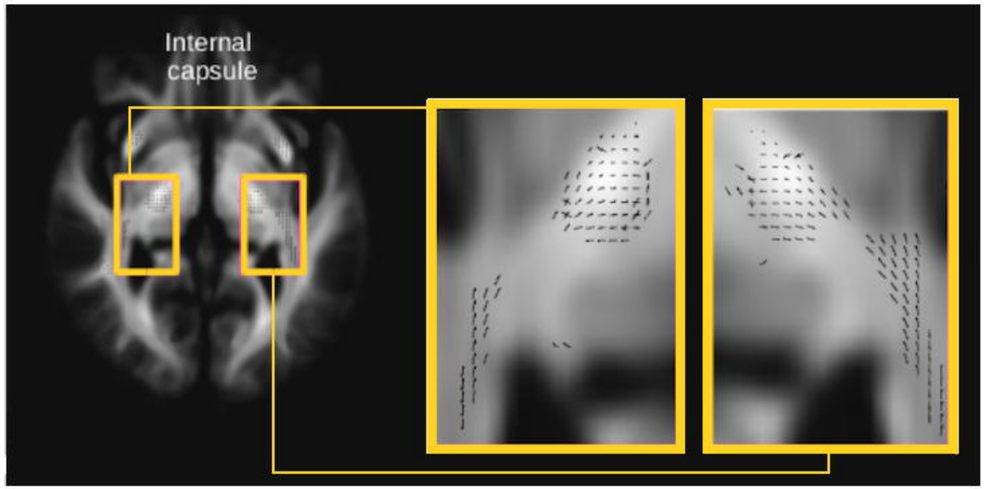

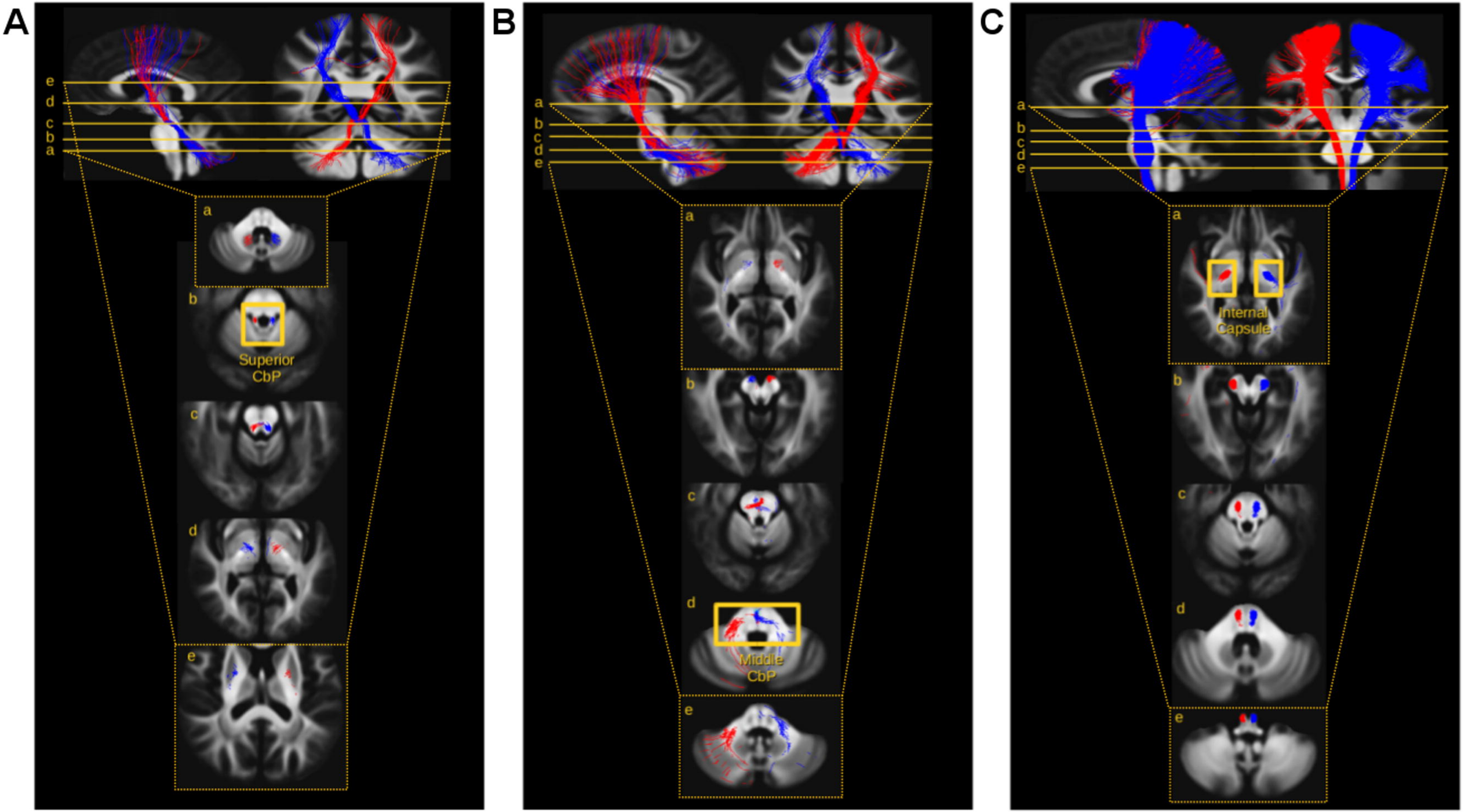
A
e
d
c
b
a
a
b
Superior
CbP
c
d
e
B
a
b
c
d
e
a
b
c
d
Middle
CbP
e
C
a
b
c
d
e
a
Internal
Capsule
b
c
d
e

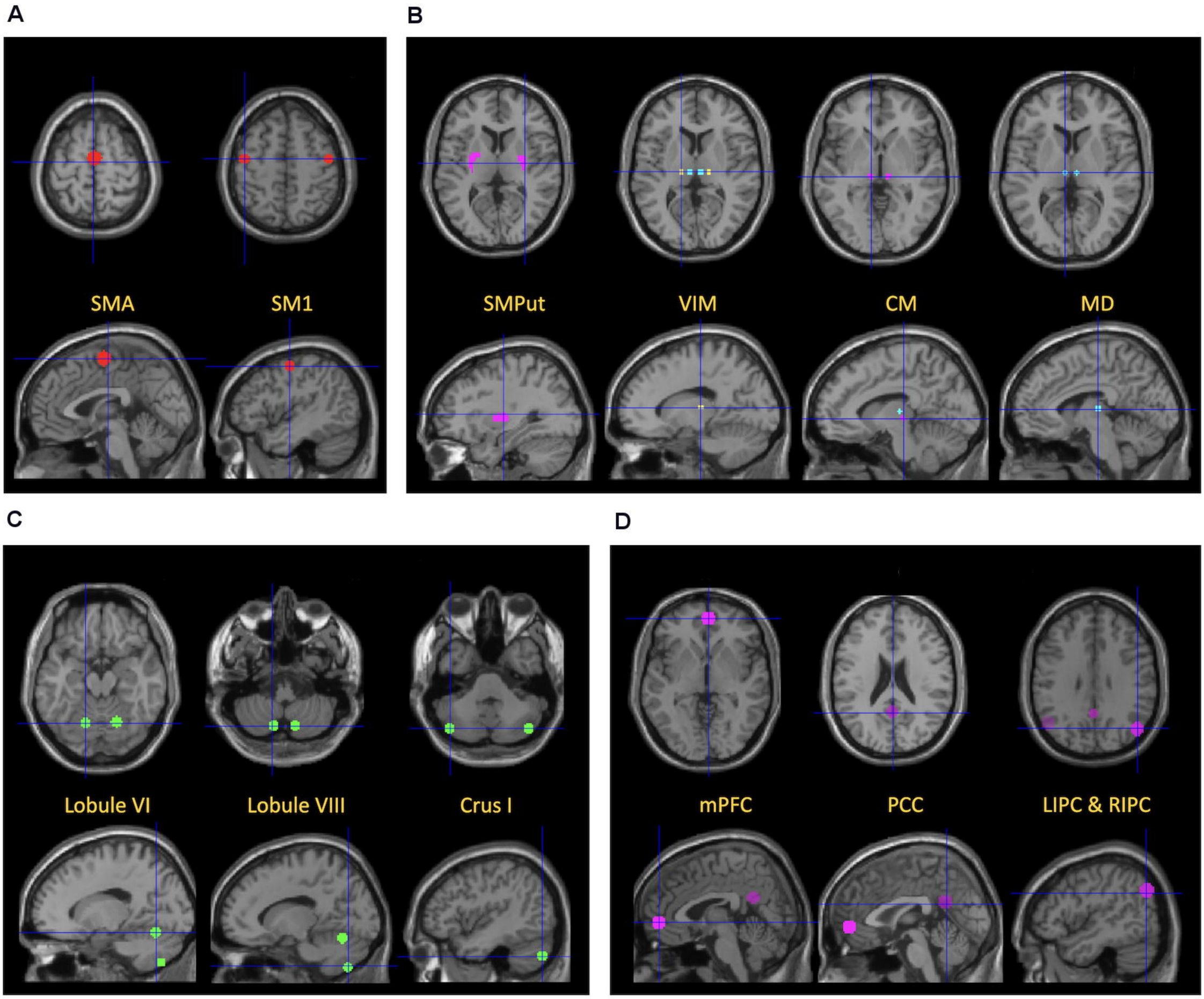
A
SMA
SM1
B
SMPut
VIM
CM
MD
C
Lobule VI
Lobule VIII
Crus I
D
mPFC
PCC
LIPC & RIPC

A

	HV	*PRRT2*	HV ≠ *PRRT2*
Cerebello-thalamo-striatal Network	SMPut — CM; Cb VIII ↻; Cb VI ↻	SMPut ← CM; Cb VIII ↻; Cb VI ↻	SMPut ← CM; Cb VIII ↻; Cb VI ↻
Cerebello-thalamo-cortical Motor Network	SMA ↻; SM1 ← VIM; Cb VIII; Cb VI ↻	SMA ↻; SM1 — VIM; Cb VIII ↻; Cb VI ↻	SMA; SM1 ← VIM; Cb VIII ↻; Cb VI
Cerebello-thalamo-prefrontal Network	mPFC ↻ — MD; Crus I ↻	mPFC ← MD; Crus I ↻	mPFC ← MD; Crus I
Default Mode Network	mPFC ↻; LIPC; RIPC; PCC	mPFC ↻; LIPC; RIPC; PCC	mPFC ↻; LIPC; RIPC; PCC

B

	SHAM	cTBS	SHAM ≠ cTBS
Cerebello-thalamo-striatal Network	SMPut ← CM; Cb VIII; Cb VI	SMPut — CM; Cb VIII ↻; Cb VI	SMPut ← CM; Cb VIII ↻; Cb VI
Cerebello-thalamo-cortical Motor Network	SMA ↻; SM1 — VIM; Cb VIII ↻; Cb VI ↻	SMA ↻; SM1 ← VIM; Cb VIII ↻; Cb VI ↻	SMA; SM1 ← VIM; Cb VIII ↻; Cb VI ↻
Cerebello-thalamo-prefrontal Network	mPFC ↻ — MD; Crus I ↻	mPFC — MD; Crus I	mPFC — MD; Crus I

C